Nucleosome Shape Dictates Chromatin Fiber Structure

Martin Depken[†‡*] and Helmut Schiessel[‡]
[†]Max Planck Institute for the Physics of Complex Systems, Dresden, Germany; and [‡]Instituut-Lorentz for Theoretical Physics, Universiteit Leiden, Leiden, The Netherlands

ABSTRACT In addition to being the gateway for all access to the eukaryotic genome, chromatin has in recent years been identified as carrying an epigenetic code regulating transcriptional activity. Though much is known about the biochemistry of this code, little is understood regarding the different fiber structures through which the regulation is mediated. Over the last three decades many fiber models have been suggested, but none are able to predict even the basic characteristics of the fiber. In this work, we characterize the set of all possible dense fibers, which includes, but is not limited to, all previously suggested structures. To guide future experimental efforts, we show which fiber characteristics depend on the underlying structure and, crucially, which do not. Addressing the predictive power of these models, we suggest a simple geometric criterion based on the nucleosome shape alone. This enables us to predict the observed characteristics of the condensed chromatin fiber, and how these change with varying nucleosome repeat length. Our approach sheds light on how the in vivo observed heterogeneity in linker lengths can be accommodated within the 30 nm fiber, and suggest an important role for nucleosome surface interactions in the regulation of chromatin structure and function.

INTRODUCTION

Because of the considerable length of the eukaryotic genome, cells face the conflicting demands of densely packing the genomic DNA into the small cell nucleus, and the need for rapid and precise access to particular sections by a host of macromolecules needed for replication, transcription, repair, etc. The cell manages this in much the same way as we solve the similar problem of information storage and access in a library: by hierarchical and highly organized folding. As in a normal library, the information is largely inaccessible when compacted, and the structure must be opened up to enable readout. This is to a large extent controlled by the histone code (1–3), which is carried mainly in covalent and reversible posttranscriptional modifications of the histones, a set of DNA-associated proteins used to condense the genetic material. This code influences the degree of compaction of the fiber, and through this the local accessibility of the genetic material and ultimately the transcriptional activity in eukaryotic cells. To gain a molecular understanding of the action of the histone code, we need to establish the nature of the hierarchical structures it regulates (4,5).

On the lowest hierarchical folding level, the primary structure is composed of a string of nucleosome core particles (NCPs) connected by short stretches of DNA. Each NCP consists of a $1\frac{3}{4}$ left-handed superhelical turn of DNA wrapped around a cylindrical aggregate of eight histone proteins (two copies each of H2A, H2B, H3, and H4) (6). In native chromatin, the additional linker histones H1 and H5 are typically bound to the portions of DNA that enter and exit the spool, bringing them together into a rigid stem structure (7). Under physiological salt concentrations, the string of nucleosomes can fold in on itself, forming a secondary structure referred to as the 30 nm fiber. Whereas the primary structure (the nucleosome) is known at atomic resolution, the three-dimensional arrangement of nucleosomes into the secondary structure (the 30 nm fiber) remains poorly understood despite three decades of experiments and model building (8). The wide range of models suggested in the literature can be divided into roughly two classes: traditional solenoid models (9) and crossed-linker models (10,11). In the solenoid models, the nucleosomes that follow each other along the DNA also stack on top of each other in a solenoidal arrangement, whereas in the crossed-linker models they sit on opposite sides of the fiber. Unfortunately, neither type of model is able to predict the optimal fiber geometry, and basic characteristics, such as the fiber diameter, are fixed by fine tuning experimentally inaccessible microscopic parameters. This lack of predictive power and the fact that many of the experiments (12–16) were likely performed on amorphous samples (17) are arguably the main reasons why the structure has remained unresolved for so long. As a first step in addressing the modeling issue, we characterize the complete set of possible fiber structures, including all major contending models and a host of structures that to date have not been considered. By this method, we show which experimentally available characteristics can be used to discern the models, and which ones cannot be used to that end.

Experimental issues involving amorphous fibers were recently overcome through the reconstitution of highly regular fibers (18,19), yielding some unexpected results. The experiments of Robinson et al. (18) are especially interesting because they were performed on comparatively long fibers, with linker histones present. They show that the fiber geometry is rather insensitive to the relative distance between the nucleosomes along the DNA, indicating that the fiber

Submitted July 22, 2008, and accepted for publication September 22, 2008.
*Correspondence: depken@pks.mpg.de
Editor: Jonathan B. Chaires.

0006-3495/09/02/0777/8 $2.00
doi: 10.1016/j.bpj.2008.09.055

structure is primarily dictated by nucleosome-nucleosome interactions and not by the DNA path. Taking inspiration from this, and the previous success of geometric arguments when applied to information-carrying structures (20), we hypothesize that the NCPs pack geometrically densely on the periphery of the fiber (8) (Fig. 1 *A*). Our approach makes the implicit assumption that the short-range attraction between NCPs (21–23) constitutes the dominant mode of interaction in dense chromatin fibers, which is then modulated by the softer contribution from the DNA linker backbone (24). In this view, the problem of determining the structure of the chromatin fiber can be divided into two parts: 1), identifying the possible dense configurations of NCPs on the periphery of the fiber; and 2), estimating the energetic contribution from the linker backbone to determine which dense structure is realized. We are then able to make definite predictions without any adjustable parameters, which are all borne out when compared with the new, regular reconstituted fibers (18,19). We further suggest additional experimental tests of our model.

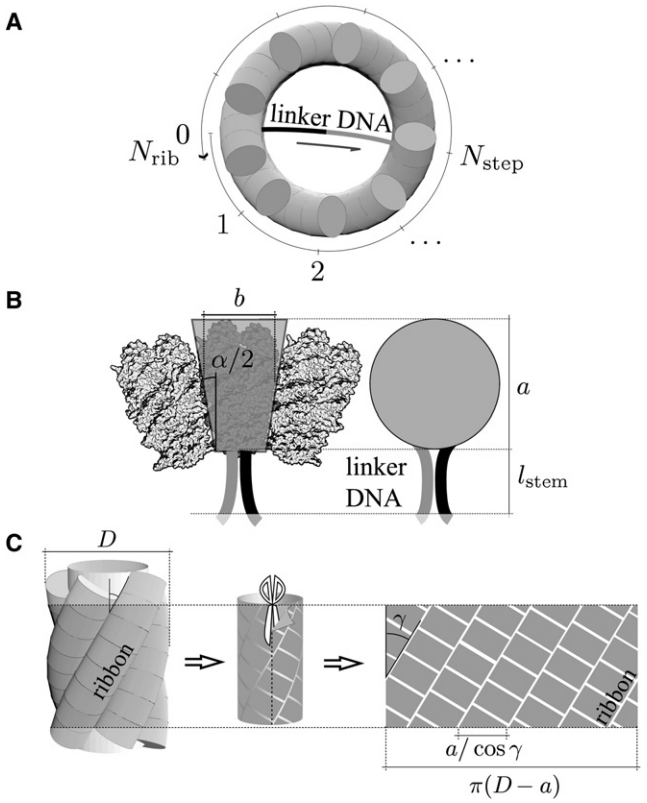

FIGURE 1 Dense chromatin fiber. (*A*) Top view of a dense fiber. The nucleosomes pack on the outside of the fiber and the linkers are situated on the inside. Here the (N_{rib}, N_{step}) = (9,4) backbone is illustrated. (*B*) Illustration of how three nucleosomes stack, and how this relates to the effective wedge shape of the nucleosome (*outlined*). By using the term ''effective wedge shape'', we stress that the nucleosome itself need not form a perfect wedge; rather, we rely on the experimental observation (25) that when nucleosomes aggregate, one can identify a wedge-shaped repeat unit. Onto the wedge-shaped cylinder we attach a rigid stem (7) to represent the ingoing and outgoing DNA and a linker histone (not shown). (*C*) Illustration of how a dense nucleosome-footprint packing on a cylinder running through the nucleosome center is a necessary condition for a dense three-dimensional structure. Also indicated are the ribbons induced by the dense packing, together with the angle γ they make with the fiber axis.

MATERIALS AND METHODS

Accounting for how NCPs aggregate in solution, we find all dense configurations of nucleosomes on the periphery of the fiber. It turns out that the set of structures is limited, and heeding some basic properties of the linker backbone severely reduces the number of possible fibers for any particular linker length. Further assuming that straight linkers are energetically favored, we derive a criterion that uniquely defines the realized fiber within the experimentally tested range, and further predict transitions in the fiber structure as the nucleosome repeat length varies.

Dense shells

Addressing the formation of a dense shell, we note that NCPs aggregate into arcs in solution (25), indicating that their wedge-shaped form (6) plays a key role in dictating large-scale arrangements of interacting nucleosomes. Drawing on this, we take the *effective* shape of the NCP as being that of a wedge-shaped cylinder (Fig. 1 *B*). It should be noted that this does not constitute an ad hoc simplification to avoid a more complicated all-atom model; rather, it is a means of accurately accounting for the way in which nucleosomes fit together when they are free to assemble under their own attractive interaction.

For nucleosomes to pack densely on the periphery of the fiber, their footprints, as marked on a cylinder inscribed through the centers of the NCPs, must also pack densely (Fig. 1 *C*). This forces the footprints into helical ribbons that wind along the fiber, formed along either footprint's symmetry axis. Some interdigitated models in the literature (18,26) belong to the set of dense packings in which the ribbons form along the major axis of the footprints (NCPs stacking side to side). Face-to-face stackings of NCPs aggregate spontaneously under the right solvent conditions (25,27), and this is also what best utilizes any short-range attractive interaction. Thus, here we assume that the NCPs stack face to face, corresponding to footprints forming ribbons along their minor axis. In the Appendix, we detail the modifications needed to treat structures with ribbons along the major axis. For a dense footprint packing, the total area of the footprints must equal the total area of the cylinder onto which they pack. This implies a linear relationship between the nucleosome line density (NLD) along the fiber σ, and the fiber diameter D:

$$\sigma = -\frac{\pi}{b} + \frac{\pi}{ab}D, \tag{1}$$

where a is the nucleosome diameter, and b is its average height (Fig. 1). This equation must be satisfied for all regular fibers, face-to-face stacked and side-to-side alike. This explains the linear correlation between diameter and NLD observed for both reconstituted and native fibers (see the Discussion for a comparison of Eq. 1 and these experiments), and offers a means of fitting back the effective nucleosome dimensions of examined fibers. Another experimentally accessible parameter (through linear dichroism on directed fibers) is the angle γ that the helical ribbons make with the fiber axis (Fig. 1 *C*). This sets the manner in which the ribbons spiral up along the fiber, and is determined by the requirement that the total number of ribbons, N_{rib}, precisely covers the periphery of the fiber (Fig. 1 *C*). This condition can be written as

$$\cos\gamma = \frac{aN_{\mathrm{rib}}}{\pi(D-a)}. \tag{2}$$

Equations 1 and 2 completely specify any dense footprint packing and constitute relations that are directly amenable to experimental tests (see

Discussion). In the Appendix, we describe how Eq. 2 is modified for the case of models with nucleosomes stacked side to side.

All the above is valid without reference to any particular effective wedge angle α (Fig. 1 *B*). Moving back to the full three-dimensional packing of nucleosomes, we see that all admissible footprint packings correspond to NCPs packed together with a specific effective wedge angle. By considering the path of the ribbons, it is straightforward to relate the effective wedge angle and the twist between nucleosomes (around the dyad axis) to the fiber diameter. Within the relevant parameter ranges, the exact expression for the wedge angle can be approximated as (see Appendix)

$$\alpha \approx \frac{2b}{D-a}\left(1-\left[\frac{aN_{\mathrm{rib}}}{\pi(D-a)}\right]^2\right), \tag{3}$$

with an accuracy of a couple of tenths of a degree. For any specific fiber diameter and number of ribbons, this directly gives the effective wedge angle, and it can easily be inverted to give the possible fiber diameters for any specific effective wedge angle. The amount of twist between neighboring nucleosome in a ribbon is given by (see Appendix)

$$\phi \approx \frac{2N_{\mathrm{rib}}ab}{\pi(D-a)^2}\sqrt{1-\left[\frac{aN_{\mathrm{rib}}}{\pi(D-a)}\right]^2}. \tag{4}$$

The two parameters α and ϕ completely specify the relative position of the nucleosomes on the periphery of a densely packed fiber, and their values can be directly compared with either experimental values (see Discussion) or results gained from optimizing the interactions in an all-atom model.

Linker paths

The above development puts no constraints on the backbone and can incorporate models with both regular and irregular backbones. We now focus on finding all possible ways in which the backbone can connect the nucleosomes in an identical fashion from nucleosome to nucleosome. Denote by N_{step} the distance across ribbons between connected nucleosomes (Fig. 1 *A*). The necessary and sufficient condition for a regular backbone winding (BW)—completely defined by the pair (N_{rib}, N_{step})—is the existence of two integers n and k such that

$$kN_{\mathrm{step}} - nN_{\mathrm{rib}} = 1, \quad 0 \le n \le k \le N_{\mathrm{rib}}. \tag{5}$$

The solution of Eq. 5 ensures that neighboring ribbons are eventually connected (after k steps and n turns; see Appendix), and hence all ribbons are visited by the backbone (unlike, e.g., the BW (4,2), which partitions the NCPs into two unconnected sets containing evenly and oddly numbered nucleosomes, respectively). The trivial BW (N_{rib}, 1) corresponds to the backbone connecting nucleosomes in neighboring ribbons ($N_{\mathrm{step}} = 1$; Fig. 1 *A*). Such a backbone can be found for fibers with any number of ribbons since with the $n = 0$ and $k = 1$, Eq. 5 is always satisfied. The classical solenoid model (9) has a (1,1) BW, and all the models considered by Wong et al. (28) also have trivial BWs. By scanning through the finite number of possible n and k values, one finds all additional nontrivial BWs, extending the set of crossed-linker models to (5,2), (7,2), (7,3), (8,3), and so on (see Table 1 for further structures and their characteristics). Thus, this approach exhaustively covers all major contending models for the fiber structure (8–10,13,14,29–31) (solenoid models, crossed-linker models, interdigitated models, etc.), including some models not previously considered. Moreover, it explains the proliferation of models and puts them all firmly within a unifying framework. This enables us to discern which observables are useful in determining the structure, and which are not. It predicts an experimentally testable, and observed, linear relationship between NLD and fiber diameter, as well as a relationship for the pitch angle for the helical nucleosome ribbons. Crucially, the relationship between the NLD and the diameter shows that these two quantities are not independent observables in dense fibers. Thus, setting the fiber diameter to a value measured in experiments, and then successfully comparing experimental values of the NLD with those calculated for a particular favorite dense microscopic model, does not constitute independent evidence for the chosen fiber structure. However, it does provide evidence that the actual structure is dense, with the effective nucleosome dimensions assumed, but it carries no further weight in determining the microscopic details of the structure. Going beyond these approaches, we now specify a microscopic criterion that leads to precise and testable predictions for the fiber structure.

TABLE 1 Characteristics of the predicted fiber structures

Structure	D (nm)	σ (1/nm)	γ deg	ϕ deg	$l_{\mathrm{repeat}}>$ bp	$l_{\mathrm{repeat}}<$ bp
$(5, 1)^+$	33	1.0	30	14	172	213
$(5, 1)^-$	33	1.0	−30	−14	172	213
$(5, 2)^+$	33	1.0	30	14	176	213
$(5, 2)^-$	33	1.0	−30	−14	176	213
$(6, 1)^+$	38	1.2	34	12	179	274
$(6, 1)^-$	38	1.2	−34	−12	178	274
$(7, 1)^+$	44	1.5	38	10	186	352
$(7, 1)^-$	44	1.5	−38	−10	184	352
$(7, 2)^+$	44	1.5	38	10	201	352
$(7, 2)^-$	44	1.5	−38	−10	200	352
$(7, 3)^+$	44	1.5	38	10	210	352
$(7, 3)^-$	44	1.5	−38	−10	209	352
$(8, 1)^+$	52	1.8	43	9	192	455
$(8, 1)^-$	52	1.8	−43	−9	191	455
$(8, 3)^+$	52	1.8	43	9	229	455
$(8, 3)^-$	52	1.8	−43	−9	228	455
$(9, 1)^+$	66	2.5	53	6	204	655
$(9, 1)^-$	66	2.5	−53	−6	202	655
$(9, 2)^+$	66	2.5	53	6	238	655
$(9, 2)^-$	66	2.5	−53	−6	236	655
$(9, 4)^+$	66	2.5	53	6	275	655
$(9, 4)^-$	66	2.5	−53	−6	275	655
$(10, 1)^+$	75	2.9	55	5	209	788
$(10, 1)^-$	75	2.9	−55	−5	207	788
$(10, 3)^+$	75	2.9	55	5	278	788
$(10, 3)^-$	75	2.9	−55	−5	277	788

Table displays all of the calculated properties of the dense fibers consistent with the structure of the nucleosome. They are (left to right): fiber structure, fiber diameter, NLD, angle formed between ribbons and fiber axis, twist between neighboring nucleosomes in the same ribbon, minimum nucleosomal repeat length, and maximum nucleosomal repeat length. The minimum repeat length differs depending on the relative helicity between the linker backbone and ribbons, indicated with a superscript + in the structure notation for the same helicity, and a superscript − for opposite helicity.

RESULTS

Realized fiber structures

Equipped with a framework that captures all possible fibers structures, and having shown that it is futile to try to discern the fiber structure by measuring the fiber diameter and NLD alone, we suggest a microscopic condition that uniquely determines which structures are realized. To be able to compare our results with the maximally dense fibers (18), we base these conditions on the known dimensions of the repeat unit for densely packed nucleosomes. Thus we use the effective NCP diameter $a = 11.5$ nm and average height $b = 6.0$ nm, as deduced for the close packings of NCPs into

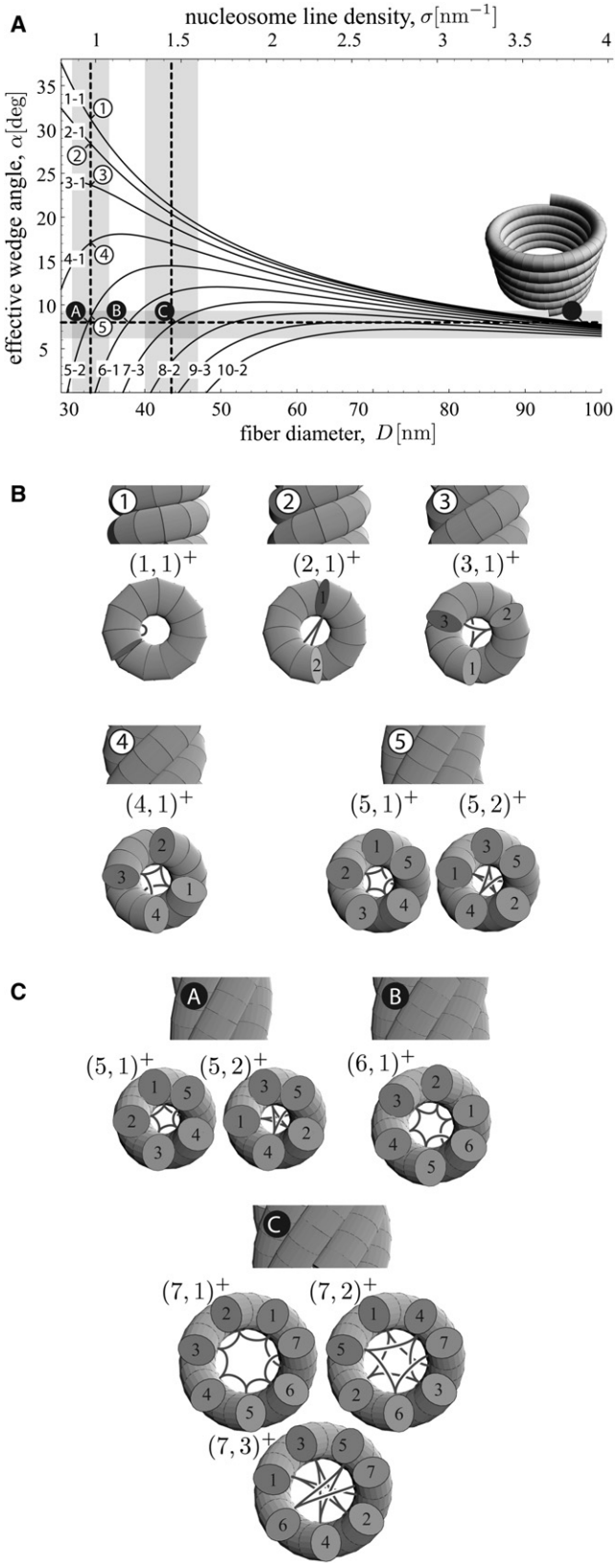

FIGURE 2 Predicted fibers. (*A*) Plot of how the effective wedge angle α varies with fiber diameter D (or equivalently, NLD σ as indicated in the upper scale of the diagram) for fibers with up to 10 ribbons (see Eq. 3). Each curve is labeled as: number of ribbons − number of possible backbones. Also indicated is the effective wedge angle measured by Dubochet and Noll (25) ($\alpha = 8^\circ$) and used in this work to predict the fiber structures. A giant fiber solution with 97 nm diameter, and similar to the tubes observed by Dubochet and Noll (25), is displayed in the inset. Further indicated are the average fiber diameters for the two different sets of fibers observed by Robinson et al. (18) (see also Fig. 3), with the area including one standard deviation indicated in gray. (*B*) All solutions with different effective wedge angles achieved by fixing the fiber diameter to 33 nm (points *1–5* in panel *A*), together with the available backbones as deduced by Eq. 5. (*C*) Some of the structures predicted by fixing the effective wedge angle to the value measured by Dubochet and Noll (25) (points *A–C* in panel *A*), together with the allowed backbones. The dimensions of the fibers with five (point *A*) and seven (point *C*) ribbons are very close to those of the structures observed by Robinson et al. (18) for dense reconstituted fibers, and furthermore are the only fibers within the error bars. This would remain true for α in the range of 6–9° (range indicated in *gray* in *A*).

columnar quasi-hexagonal crystals (27) under physiological salt concentrations and moderate pressures. We are ultimately interested in the in vivo situation where there are additional linker histones present, bringing the ingoing and outgoing DNA at each nucleosome into a stem structure (7) (Fig. 1 *B*). Letting $l_{\mathrm{stem}} = 3$ nm be the length of the induced stem, as measured by Bednar et al. (7), here we only consider fibers that satisfy $D > 2(l_{\mathrm{stem}} + a) = 29$ nm to avoid steric interactions between stems on opposite sides of the fiber.

In Fig. 2 *A* we show how, according to Eq. 3, the effective wedge angle varies with fiber diameter for fibers with up to 10 ribbons. If we were to fix the fiber diameter to some observed value (as done, e.g., by Wong et al. (28)), say 33 nm, we get a host of possible fibers (numbered 1–5 in Fig. 2, *A* and *B*). They include the solenoid model (1,1) (9), the two-start helix (2,1) (19), and the crossed-linker model (5,2) (10). The number of available structures makes it explicitly clear that the standard approach of imposing the fiber diameter tells us little about the internal structure of the fiber. It further explains the wide range of models suggested in the literature, all of which are consistent with the experimental findings but have little predictive power. Here we instead take a reductionist approach and enforce the microscopic condition of optimal dense face-to-face stacking of nucleosomes. In experiments by Dubochet and Noll (25), unconstrained nucleosomal arcs were observed with the effective wedge angle $\alpha = 8^\circ$ for the NCP repeat unit. This will be the effective wedge angle assumed throughout the rest of this article, though we will show that the end result is quite insensitive to the precise value assumed. With this microscopic condition we directly get a discrete set of possible shell structures, three of which are shown in Fig. 2 *C* (structures *A–C*), and all of which are clearly distinguished from each other on the level of the fiber diameter and NLD (see Table 1). Here we do not discuss the very wide fibers, one of which is displayed in the inset of Fig. 2 *A*. These structures may never be realized in chromatin, but are similar to the gigantic tubes of NCPs observed by Dubochet and Noll (25). The results of the simple

assumption of a dense packing of nucleosomal wedges are summarized in Table 1, where we list all fibers with a fiber diameter up to 75 nm. As detailed below, some of these have already been observed, whereas others might still be found through further experiments.

We now examine the linker backbone to determine which one of the above structures is realized for any specific nucleosomal repeat length. Though we lack a precise model for the energetics of the backbone, we can still put lower and upper bounds on the possible repeat lengths for a specific shell structure and BW. The lower bound is set by the shortest distance between two successive stems along the backbone, assuming that 165 basepairs are contained between the entrance and exit points of a stem. This depends not only on the BW $(N_{\mathrm{rib}}, N_{\mathrm{step}})$ but also on the relative helicity of backbone and ribbons. In Table 1 we denote structures in which ribbons and backbone have the same helicity by $(N_{\mathrm{rib}}, N_{\mathrm{step}})^{+}$, and by $(N_{\mathrm{rib}}, N_{\mathrm{step}})^{-}$ in the opposite case. The upper limit for the linker length is set by the excluded volume constraint on the inside of the fiber. We assume that due to the presence of cationic histone tails, the highly charged linker DNA can be densely packed, limited by a hexagonal packing with a center-to-center distance set by the DNA diameter $d_{\mathrm{DNA}} = 2$ nm. Thus we account for the most general and basic properties of the linker backbone, and the resulting limits on the linker lengths are indicated in Table 1.

We see that for the shortest repeat lengths the realized structure must always be $(5,1)^{\pm}$ or $(5,2)^{\pm}$, which feature the 33 nm diameter that gives these structures their name. Of these two structures, we expect $(5,2)^{\pm}$ to be realized because it allows for the straightest linkers (Fig. 2 *C*, structure *A*). When the linker length is increased, the central core of the fiber eventually becomes too crowded to house all the linker DNA, and the fiber must take on a larger structure before the maximum repeat length of 213 bp is reached. The fact that $(7,3)^{\pm}$ (possible for repeat lengths $>$ 209 bp) has the straightest linkers (Fig. 2 *C*, structure *C*) makes it a good candidate for the target structure. By assuming that straight linkers are favored, we go one step further and use a rudimentary model of the linker energy, including contributions from bending. Thus, through the simple geometric and microscopic condition of an optimal nucleosome packing combined with rudimentary arguments concerning the energetics of the backbone, the model predicts a transition in fiber diameter (33–44 nm) and NLD (1.0–1.5 nm^{-1}) for nucleosome repeat lengths somewhere in the range of 209–213 bp.

DISCUSSION

Having discussed the theoretically possible fibers for different repeat lengths and identified a transition point between structures, we now compare these findings with recent results on dense reconstituted fibers. Robinson et al. (18) observed that such fibers clustered into two sets, each signified by a specific fiber diameter and NLD (Fig. 3). As pointed out

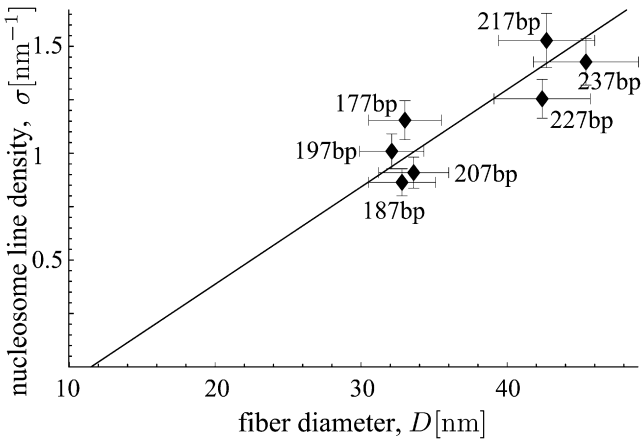

FIGURE 3 Experimental observations on dense fibers. Re-representation of data published by Robinson et al. (18) for reconstituted fibers with different nucleosomal repeat lengths (indicated). The data points cluster around two specific diameters (D = 33 nm and 44 nm) and nucleosome line densities ($\sigma = 1.0\ \mathrm{nm}^{-1}$ and $1.4\ \mathrm{nm}^{-1}$). The error bars indicate one standard deviation. Also shown is the linear relation between fiber diameter and NLD predicted by our model (Eq. 1), using the nucleosome dimensions determined by Mangenot et al. (27). It is consistent with both thin and thick fibers, without any adjustable parameters. The linear relation conversely can be used to determine the nucleosome dimensions from the data. If we perform a simple least-square fit to the points in the graph, we arrive at the effective dimensions $a = 11.4$ nm and $b = 7.2$ nm for the repeat unit.

by Wong et al. (28), a similar clustering is seen for the native fibers examined by Williams et al. (13). Because the fiber diameter and the NLD are linearly related through condition Eq. 1, we can use this as a direct test of our approach. In Fig. 3, we plot this relation together with the observed fiber diameter and nucleosome line densities (18). Our model is in good agreement with the experimental data, and manages to account for both thin and thick fibers without any fit parameters. (Alternatively, one could use the data to fit back the nucleosome dimensions, and a simple-minded least-square fit to the points in Fig. 3 gives the nucleosome dimensions $a = 11.4$ nm and $b = 7.2$ nm.) The fact that these regular fibers all fall close to the predicted line is evidence that they are very densely packed—something that is achieved only by the nucleosomes forming ribbons on the periphery of the fiber. A linear relationship between NLD and fiber diameter for fibers at different salt and magnesium concentrations has also been observed in chicken erythrocyte chromatin (32). A direct comparison with Eq. 1 cannot be made, since the experiments did not allow for a direct measure of the fiber diameter. However, the linear correlation observed indicates that these fibers also form regular nucleosome shells, although the packing may result in different effective dimensions of the repeat unit.

In Fig. 2 *A* we indicate the average diameters of the two clusters observed by Robinson et al. (18) (33 and 44 nm). The structures predicted by our model (Fig. 2, *A* and *C*, structures *A* and *C*) are the only fibers within the error bars of the experiments. It can also be seen that these predictions are

rather robust against changes in the effective wedge angle (a wedge angle between 6° and 9° would yield the same structures). In addition, a transition between these fiber structures was observed somewhere between repeat lengths of 207 and 217 bp, which is also captured by our model.

Apparently contradicting these results is another recent set of experiments on regular fibers suggesting a two-ribbon structure (19). These experiments were performed on short fibers (10–12 nucleosomes), and thus it is unlikely that they would be able to capture the structures suggested here (five and seven ribbons). Such structures would only stack about two nucleosomes per ribbon and expose about half of the nucleosome faces to the solution, rendering them energetically unfavorable. In line with our assumption that nucleosome interactions drive the assembly of the fiber, we expect short fibers to favor fewer ribbons to minimize the number of nucleosome faces exposed to the solution. The same reasoning applies to inferring the fiber organization from the crystallographic structure of the tetra-nucleosome (33), which renders both of these approaches unsuitable to test our assumption of a close face-to-face stacking of nucleosomes. Though these structures are unlikely to be energetically favored for longer fibers, they are still regular and can be described by our approach as (2,1) structures, albeit with different effective dimensions for the nucleosome, and with a different wedge angle than the one used here to describe maximally dense fibers.

We also wish to point to a very recent study (M. Kruithof, F.-T. Chan, A. Routh, C. Logie, D. Rhodes, and J. van Noort, unpublished results) in which fibers with 25 nucleosomes and a repeat length of 197 bp were prestretched and manipulated by magnetic tweezers. The fibers were found to be much softer than one would naively expect from the structures we argue for here, but this might still be accounted for by the fact that the attained fiber structure may be sensitive to the folding procedure.

Our model could readily be tested with some of the techniques already applied to more amorphous fibers; for example, linear dichroism (15,16) could be used to determine the ribbon angle γ for these newly available fibers, offering a direct test by Eq. 2 (see Table 1). It would also be interesting to see whether structures such as $(8,3)^{\pm}$ and $(9,4)^{\pm}$ are ever realized for repeat lengths longer than those investigated by Robinson et al. (18). Our results further highlight the importance of surface structure and interactions in the formation of the chromatin fiber. This is in accord with recent studies of fibers containing the evolutionary conserved histone variant H2A.Z, which displays changes in the nucleosome surface structure and is implicated in the formation of hetrochromatin (34,35). Another property of in vivo fibers that finds a natural explanation in our approach is the observed heterogeneity of the nucleosome repeat unit (36). Within our model, this is to be expected since the overall structure is dominated by nucleosome interactions, and, as shown above, rather insensitive to variations of the linker length. In fact, essentially all the variation seen in linker lengths in vivo (37) is contained in the range of 176–213 bp. This suggests that in vivo the (5,2) structure is predominant, with a few cell types displaying the larger (7,3) structure.

With the inclusion of a more detailed energetic model for the linker backbone, the above development should form the basis for statistical and kinetic studies of how in vivo variations and correlations in repeat length affect the locally realized structure, its stability toward posttranscriptional modifications of the nucleosome, and thus the in vivo condensation-decondensation transition of the 30 nm fiber. In vitro, this transition can be probed by a change of ionic conditions (7) or the application of a sufficiently large external force, e.g., in single-molecule experiments using optical or magnetic tweezers (38). In vivo, this can be done by the acetylation of histone tails (3,39), which offers a straightforward means of increasing accessibility to the packed genetic material. Understanding the densest structure of the chromatin fiber now opens the door to detailed study of this important regulatory mechanism and its connection to the histone code (1–3). We hope that the work presented here will help guide future experimental studies, and that the structural insights thus gained will facilitate a comprehensive understanding of the subtle interplay between structure and function in chromatin (4). Lastly, we speculate that the extraordinary evolutionary conservation enjoyed by the nucleosome is to a large degree necessitated by the fact that its detailed and tunable surface structure is crucial for correct folding at the level of the 30 nm fiber. Through our requirement of a dense face-to-face stacking of the nucleosomes, this is essentially also the underlying assumption of our work. The parallels with the geometric nature of Watson-Crick basepairing (20) at the fundamental level of information-carrying structures in the same physical object are also clear.

APPENDIX

Here we detail the derivations omitted in previous sections. We show how to find all possible (regular) BWs, how to calculate the wedge and twist angle for nucleosomes, and how things should be modified to cover models in which the nucleosomes stack side to side.

Backbone winding

Building on the footprint packings displayed in Fig. 4, define the vector $\underline{p}_{\text{top}}$ as the vector connecting the nucleosome at its base with the next nucleosome (along the backbone) in the same ribbon. In a similar manner, define $\underline{p}_{\text{side}}$ as ending at the next nucleosome encountered in the ribbon neighboring to the right. Let k_{top} be the number of steps taken along the backbone when going between the nucleosomes connected by $\underline{p}_{\text{top}}$, and n_{top} the number of times the fiber was circled in doing so. Define k_{side} and n_{side} in an analogous manner. Then, on our strip of footprints we have

$$\underline{p}_{\text{top}} = \left\{k_{\text{top}}\Delta - \pi(D-a)n_{\text{top}}\right\}\underline{e}_{\theta} + \frac{k_{\text{top}}}{\sigma}\underline{e}_{z},$$

$$\underline{p}_{\text{side}} = \left\{k_{\text{top}}\Delta - \pi(D-a)n_{\text{side}}\right\}\underline{e}_{\theta} + \frac{k_{\text{side}}}{\sigma}\underline{e}_{z},$$

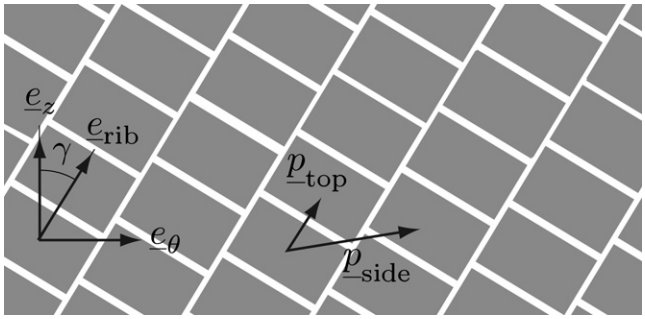

FIGURE 4 Footprint packing structure. The footprint packing defined in Fig. 1 *C*, with lattice vectors $\underline{p}_{\mathrm{top}}$ and $\underline{p}_{\mathrm{side}}$ indicated, together with the unit vectors $\underline{e}_z$, $\underline{e}_\theta$, and $\underline{e}_{\mathrm{rib}}$.

where σ is the NLD along the fiber (thus $1/\sigma$ is the specific distance along the fiber for each nucleosome), and Δ is the circumferential distance between nucleosomes following each other along the backbone. For the packing of ribbons to be dense, the parallelogram spanned by these two vectors must be of the same area as the footprint:

$$ab = \left|\underline{p}_{\mathrm{side}} \hat{} \underline{p}_{\mathrm{top}}\right| = \pi(D-a)\left|n_{\mathrm{top}}k_{\mathrm{side}} - n_{\mathrm{side}}k_{\mathrm{top}}\right|/\sigma.$$

Using Eq. 1, and fixing the reference helicity of backbone and ribbons, this becomes

$$n_{\mathrm{top}}k_{\mathrm{side}} - n_{\mathrm{side}}k_{\mathrm{top}} = 1.$$

The solution to this simple relationship gives all possible backbone structures. It can further be put in terms of N_{rib}, N_{step} as follows: Before returning to the starting ribbon when walking along the backbone, all ribbons traversed on the outside of the fiber in the first step have to be visited exactly once (ribbon 1, 2, …, $N_{\mathrm{step}} - 1$ of Fig. 1 *A*). This can only be done during successive turns around the fiber, and thus $N_{\mathrm{step}} = n_{\mathrm{top}}$. Also, before returning to the same ribbon, all other ribbons must be visited exactly once, giving $k_{\mathrm{top}} = N_{\mathrm{rib}}$. This gives Eq. 5.

Nucleosome wedge angle and ribbon torsion

The center line of each nucleosome ribbon winding up the fiber can be described by the space curve

$$\underline{r}(s) = \frac{D-a}{2}\left(\underline{e}_r + \frac{\theta(s)}{\tan\gamma}\,\underline{e}_z\right), \quad \theta(s) = \frac{2s\sin\gamma}{D-a} + \theta_0,$$

where s is the arch length of the curve, and θ_0 is a constant depending on which ribbon is under consideration. The Frenet vectors (40) for this curve are given by

$$\underline{e}_1 = \underline{e}_{\mathrm{rib}} = \sin\gamma\,\underline{e}_\theta + \cos\gamma\,\underline{e}_z,$$
$$\underline{e}_2 = \frac{\partial\underline{e}_1}{\partial s}\Big/\left\|\frac{\partial\underline{e}_1}{\partial s}\right\| = -\underline{e}_r,$$
$$\underline{e}_3 = \underline{e}_1 \hat{} \underline{e}_2 = -\cos\gamma\,\underline{e}_\theta + \sin\gamma\,\underline{e}_z.$$

From this the curvature κ (inverse radius of curvature) and torsion τ are given by (40)

$$\kappa = \frac{\partial\underline{e}_1}{\partial s}\cdot\underline{e}_2 = \frac{2\sin^2\gamma}{D-a}, \quad \tau = \frac{\partial\underline{e}_2}{\partial s}\cdot\underline{e}_3 = \frac{2\sin\gamma\cos\gamma}{D-a}.$$

Because each nucleosome covers an approximate distance b along the curve, the wedge angle α and twist between nucleosomes ϕ can in turn be approximated by

$$\alpha \approx b\kappa = \frac{2b\sin^2\gamma}{D-a}, \quad \phi \approx b\tau = \frac{2b\sin\gamma\cos\gamma}{D-a}.$$

For the case of face-to-face stackings, Eq. 2 can be used to eliminate γ, with the result displayed in Eqs. 3 and 4.

Side-to-side stackings

For the models in which nucleosomes stack side to side, all the above goes through unchanged, with the only modification that the space curves (kept parallel with the nucleosome dyad axis) $\underline{r}(s)$ are now perpendicular to the ribbons at every point. The result for the wedge angle remains the same, whereas ϕ can no longer be interpreted as the twist around the dyad axis between nucleosomes in the same ribbon. For these models, Eq. 2 is replaced by

$$\sin\gamma = \frac{bN_{\mathrm{rib}}}{\pi(D-a)},$$

resulting in

$$\alpha \approx \frac{2b^3N_{\mathrm{rib}}^2}{\pi^2(D-a)^3},$$

with the use of Eq. 2.

We thank Ralf Everaers, Nima Hamedani Radja, Marc Emanuel, Andreas Henriksson, and John van Noort for fruitful discussions, and Eric Galburt, Stephan Grill, and Mirjam Mayer for insightful comments on the manuscript. We especially thank Wim van Saarloos, without whom this research would not have been possible.

M.D. acknowledges support from the Foundation for Fundamental Research on Matter and the Max Planck Society.

REFERENCES

1. Strahl, B., and C. Allis. 2000. The language of covalent histone modifications. *Nature*. 403:41–45.
2. Jenuwein, T., and C. Allis. 2001. Translating the histone code. *Sci. STKE*. 293:1074–1080.
3. Dion, M., S. Altschuler, L. Wu, and O. Rando. 2005. Genomic characterization reveals a simple histone H4 acetylation code. *Proc. Natl. Acad. Sci. USA*. 102:5501–5506.
4. Kornberg, R. D., and Y. Lorch. 2007. Chromatin rules. *Nat. Struct. Mol. Biol.* 14:986–988.
5. Tremethick, D. J. 2007. Higher-order structures of chromatin: the elusive 30 nm fiber. *Cell*. 128:651–654.
6. Luger, K., A. W. Mäder, R. K. Richmond, D. F. Sargent, and T. J. Richmond. 1997. Crystal structure of the nucleosome core particle at 2.8 Å resolution. *Nature*. 389:251–260.
7. Bednar, J., R. A. Horowitz, S. A. Grigoryev, L. M. Carruthers, J. C. Hansen, et al. 1998. Nucleosomes, linker DNA, and linker histone form a unique structural motif that directs the higher-order folding and compaction of chromatin. *Proc. Natl. Acad. Sci. USA*. 95: 14173–14178.
8. van Holde, K., and J. Zlatanova. 2007. Chromatin fiber structure: where is the problem now? Semin. Cell Dev. Biol. 18:651–658.
9. Finch, J. T., and A. Klug. 1976. Solenoidal model for superstructure in chromatin. *Proc. Natl. Acad. Sci. USA*. 73:1897–1901.
10. Woodcock, C. L., S. A. Grigoryev, R. A. Horowitz, and N. Whitaker. 1993. A chromatin folding model that incorporates linker variability

generates fibers resembling the native structures. *Proc. Natl. Acad. Sci. USA.* 90:9021–9025.

11. Bednar, J., R. A. Horowitz, J. Dubochet, and C. L. Woodcock. 1995. Chromatin conformation and salt-induced compaction: three-dimensional structural information from cryoelectron microscopy. *J. Cell Biol.* 131:1365–1376.
12. Widom, J., J. T. Finch, and J. O. Thomas. 1985. Higher-order structure of long repeat chromatin. *EMBO J.* 4:3189–3194.
13. Williams, S. P., B. D. Athey, L. J. Muglia, R. S. Schappe, A. H. Gough, et al. 1986. Chromatin fibers are left-handed double helices with diameter and mass per unit length that depend on linker length. *Biophys. J.* 49:233–248.
14. Worcel, A., S. Strogatz, and D. Riley. 1981. Structure of chromatin and the linking number of DNA. *Proc. Natl. Acad. Sci. USA.* 78:1461–1465.
15. McGhee, J. D., J. M. Nickol, G. Felsenfeld, and D. C. Rau. 1983. Higher order structure of chromatin: orientation of nucleosomes within the 30 nm chromatin solenoid is independent of species and spacer length. *Cell.* 33:831–841.
16. Sen, D., S. Mitra, and D. M. Crothers. 1986. Higher-order structure of chromatin: evidence from photochemically detected linear dichroism. *Biochemistry.* 25:3441–3447.
17. van Holde, K. E., and J. Zlatanova. 1995. Chromatin higher order structure: chasing a mirage? J. Biol. Chem. 270:8373–8376.
18. Robinson, P. J. J., L. Fairall, V. A. T. Huynh, and D. Rhodes. 2006. EM measurements define the dimensions of the ''30-nm'' chromatin fiber: evidence for a compact, interdigitated structure. *Proc. Natl. Acad. Sci. USA.* 103:6506–6511.
19. Dorigo, B., T. Schalch, A. Kulangara, S. Duda, R. R. Schroeder, et al. 2004. Nucleosome arrays reveal the two-start organization of the chromatin fiber. *Science.* 306:1571–1573.
20. Watson, J., and F. Crick. 1953. Molecular structure of nucleic acids. *Nature.* 171:737–738.
21. Mangenot, S., A. Leforestier, P. Vachette, D. Durand, and F. Livolant. 2002. Salt-induced conformation and interaction changes of nucleosome core particles. *Biophys. J.* 82:345–356.
22. Mangenot, S. 2002. Interactions between isolated nucleosome core particles: a tail-bridging effect? The Eur. Phys. J. E Soft Matter. 7:221–231.
23. Mühlbacher, F., H. Schiessel, and C. Holm. 2006. Tail-induced attraction between nucleosome core particles. *Phys. Rev. E Stat. Nonlin. Soft Matter Phys.* 74:031919.
24. Mergell, B., R. Everaers, and H. Schiessel. 2004. Nucleosome interactions in chromatin: fiber stiffening and hairpin formation. *Phys. Rev. E Stat. Nonlin. Soft Matter Phys.* 70:011915.
25. Dubochet, J., and M. Noll. 1978. Nucleosome arcs and helices. *Science.* 202:280–286.
26. Robinson, P. J. J., and D. Rhodes. 2006. Structure of the '30 nm' chromatin fibre: a key role for the linker histone. *Curr. Opin. Struct. Biol.* 16:336–343.
27. Mangenot, S., A. Leforestier, D. Durand, and F. Livolant. 2003. Phase diagram of nucleosome core particles. *J. Mol. Biol.* 333:907–916.
28. Wong, H., J. -M. Victor, and J. Mozziconacci. 2007. An all-atom model of the chromatin fiber containing linker histones reveals a versatile structure tuned by the nucleosomal repeat length. *PLoS ONE.* 2:e877.
29. Makarov, V., S. Dimitrov, V. Smirnov, and I. Pashev. 1985. A triple helix model for the structure of chromatin fiber. *FEBS Lett.* 181: 357–361.
30. Daban, J. R., and A. Bermúdez. 1998. Interdigitated solenoid model for compact chromatin fibers. *Biochemistry.* 37:4299–4304.
31. Schiessel, H., W. M. Gelbart, and R. Bruinsma. 2001. DNA folding: structural and mechanical properties of the two-angle model for chromatin. *Biophys. J.* 80:1940–1956.
32. Gerchman, S. E., and V. Ramakrishnan. 1987. Chromatin higher-order structure studied by neutron scattering and scanning transmission electron microscopy. *Proc. Natl. Acad. Sci. USA.* 84:7802–7806.
33. Schalch, T., S. Duda, D. F. Sargent, and T. J. Richmond. 2005. X-ray structure of a tetranucleosome and its implications for the chromatin fibre. *Nature.* 436:138–141.
34. Fan, J. Y., D. Rangasamy, K. Luger, and D. J. Tremethick. 2004. H2A.Z alters the nucleosome surface to promote HP1alpha-mediated chromatin fiber folding. *Mol. Cell.* 16:655–661.
35. Zlatanova, J., and A. Thakar. 2008. H2A.Z: view from the top. *Structure.* 16:166–179.
36. Holde, K. E. V. 1988. Chromatin. Springer, London.
37. Widom, J. 1992. A relationship between the helical twist of DNA and the ordered positioning of nucleosomes in all eukaryotic cells. *Proc. Natl. Acad. Sci. USA.* 89:1095–1099.
38. Cui, Y., and C. Bustamante. 2000. Pulling a single chromatin fiber reveals the forces that maintain its higher-order structure. *Proc. Natl. Acad. Sci. USA.* 97:127–132.
39. Horn, P., and C. Peterson. 2002. Chromatin higher order folding–wrapping up transcription. *Science.* 297:1824–1827.
40. Valiron, G. 1986. The Classical Differential Geometry of Curves and Surfaces. Math Sci Press, Brookline, MA.